Applied Surface Science 387 (2016) 857–863

Contents lists available at ScienceDirect

Applied Surface Science

journal homepage: www.elsevier.com/locate/apsusc

Porous carbon with a large surface area and an ultrahigh carbon purity via templating carbonization coupling with KOH activation as excellent supercapacitor electrode materials

Fei Sun, Jihui Gao*, Xin Liu, Xinxin Pi, Yuqi Yang, Shaohua Wu

School of Energy Science and Engineering, Harbin Institute of Technology, Harbin 150001, China

ARTICLE INFO

Article history:
Received 20 March 2016
Received in revised form 6 June 2016
Accepted 28 June 2016
Available online 29 June 2016

Keywords:
Carbon materials
MgO template
Hierarchical pore
Supercapacitor
Carbon purity

ABSTRACT

Large surface area and good structural stability, for porous carbons, are two crucial requirements to enable the constructed supercapacitors with high capacitance and long cycling lifespan. Herein, we successfully prepare porous carbon with a large surface area (3175 $m^2 g^{-1}$) and an ultrahigh carbon purity (carbon atom ratio of 98.25%) via templating carbonization coupling with KOH activation. As-synthesized MTC-KOH exhibits excellent performances as supercapacitor electrode materials in terms of high specific capacitance and ultrahigh cycling stability. In a three electrode system, MTC-KOH delivers a high capacitance of 275 F g^{-1} at 0.5 A g^{-1} and still 120 F g^{-1} at a high rate of 30 A g^{-1}. There is almost no capacitance decay even after 10,000 cycles, demonstrating outstanding cycling stability. In comparison, pre-activated MTC with a hierarchical pore structure shows a better rate capability than microporous MTC-KOH. Moreover, the constructed symmetric supercapacitor using MTC-KOH can achieve high energy densities of 8.68 Wh kg^{-1} and 4.03 Wh kg^{-1} with the corresponding power densities of 108 W kg^{-1} and 6.49 kW kg^{-1}, respectively. Our work provides a simple design strategy to prepare highly porous carbons with high carbon purity for supercapacitors application.

1. Introduction

Supercapacitors, due to their high power density (10^3–10^4 W kg^{-1}) and long cycling life (>100,000 cycles), have been extensively studied and applied for portable electronic devices [1–3]. Porous carbons have attracted great attention as electrode materials of supercapacitors because of their high surface area, chemical inertness and good thermal and mechanical stability [4,5]. The current electrode materials used for supercapacitors, especially electrical double layer capacitors (EDLCs) are mainly activated carbons prepared from various type of biomass. Despite the relatively high capacitance at low rate, the capacitance rapidly deteriorates at high rates due to the inefficient ion transport in the tortuous and unordered microporous channels [6].

In contrast, silica based template methods have been explored to design ordered mesoporous porous carbon with desirable pore structure for supercapacitor use. However, the template removal usually requires the employment of corrosive acids, making industrial-level production difficult [7]. Recently, various salt or metal oxide tempalte methods which employ ZnO [8], Na_2CO_3 [9], MgO [10–13], and $CaCO_3$ [14] as pore creating agents have been reported for preparing porous carbons. Among these templates, MgO was denmonstrated to be ideal due to the structure stability, no reaction with carbon during carbonization process, and easily dissolving into diluted acidic solution [10].

In the present work, we employed magnesium nitrate as template through one-step carbonization process to synthesize the MgO-templated porous carbon (MTC). To further improve the porosity of MTC, KOH activation with a low KOH dose was conducted to produce the MTC-KOH sample. Impressively, as-prepared MTC-KOH shows characteristics of highly porous structure with surface area up to 3175 $m^2 g^{-1}$ and ultralow heteroatom content with carbon percentage up to 98.25 atom%. The unique microstructure endows MTC-KOH with outstanding capacitive performances, delivering a high capacitance of 275 F g^{-1} at 0.5 A g^{-1} and still maintaining 120 F g^{-1} at high rate of 30 A g^{-1}. Moreover, the fabricated symmertric supercapacitors can also achieve high energy densies and power densities, demonstrating the excellent device performance.

* Corresponding author.
E-mail address: gaojh@hit.edu.cn (J. Gao).

http://dx.doi.org/10.1016/j.apsusc.2016.06.176
0169-4332/

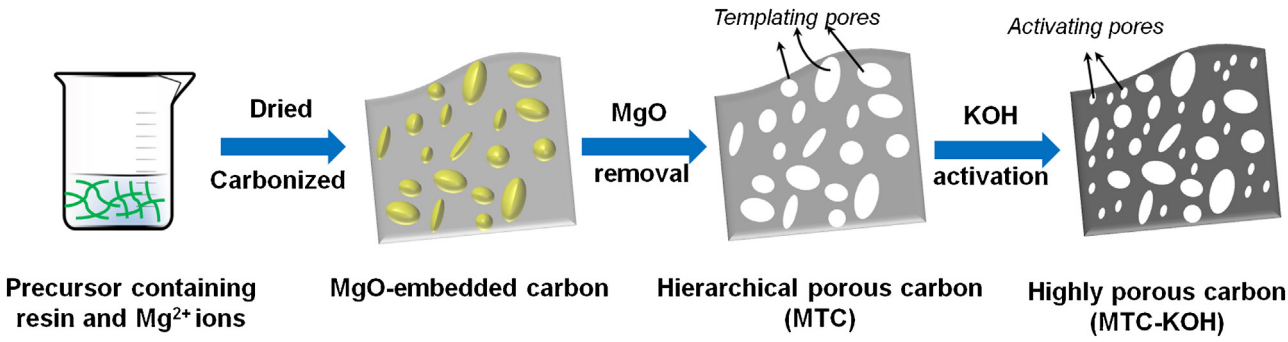

Fig. 1. Schematic illustration of the synthesis process of hierarchically porous carbon and highly porous carbon.

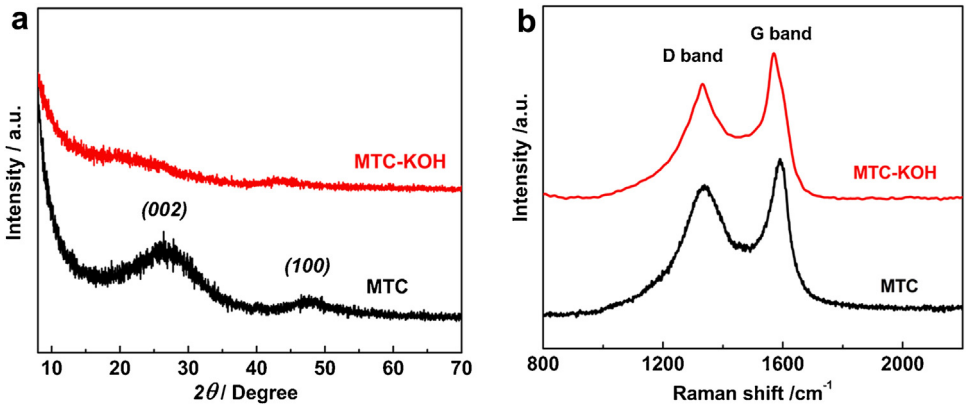

Fig. 2. (a) XRD patterns of MTC and MTC-KOH; (b) Raman spectra of MTC and MTC-KOH.

2. Materials and methods

2.1. Sample preparation

For the synthesis of MgO-templated porous carbon (MTC), 5 g phenolic resin were firstly dissolved in 20 mL anhydrous ethanol under vigorous stirring. At the same time, 5 g Magnesium nitrate hexahydrate (Mg $(NO_3)_2{\cdot}6H_2O$) were mixed with 20 g deionized water and 50 g 10 wt% NaOH solution. After drying, the homogeneous mixture was heat-treated in furnace with a heating rate of 5 °C min^{-1} up to 900 °C in a nitrogen atmosphere and held for 3 h to obtain the products. Subsequent washing by hydrochloric acid and water removed the MgO template. The washed products were then dried in vacuum at 120 °C for 12 h for characterization. To investigate the influence of carbonization temperature on carbon structure, sample MTC-2 (with carbonization temperature of 800 °C) and MTC-3 (with carbonization temperature of 700 °C) were also prepared and characterized.

For the synthesis of MTC-KOH sample, MTC and KOH were mixed and grinded with mass ratio of 1:1 to get the mixture of MTC and KOH. The mixture was activated under 900 °C and experience the same washing and drying procedures as MTC to yield the highly porous MTC-KOH sample.

2.2. Characterization

MTC and MTC-900 were analyzed using transmission electron microscopy (TEM, JEOL-2010) to investigate the microstructure. The pore structure characteristics were determined by N_2 adsorption at −196 °C using ASAP 2020 volumetric sorption analyzer. X-ray photoelectron spectroscopy (XPS) analysis was performed on a PHI 5700 ESCA system using AlKa X-ray at 14 kV and 6 mA. X-ray diffraction (XRD) measurements were examined on a Rigaku D/Max 2400 diffractometer by using Cu Ka radiation (40 kV, 100 mA, λ = 1.5406 Å). Raman spectroscopy was examined on a Renishaw inVia Micro-Raman spectrometer at 532 nm.

2.3. Preparation of electrode and electrochemical measurement

A three-electrode configuration, using 6 M KOH as the electrolyte, was constructed to evaluate the supercapacitive performance of the prepared samples. The working electrodes were prepared by mixing the active materials with conducting carbon black and binder poly-tetrafluoroethylene (PTFE) with the weight ratio of 8:1:1. Nickel-foam was used as current collector. The active material on each electrode was ~3.2 mg. Pt slice and a saturated calomel electrode (SCE) were used as the counter electrode and reference electrode, respectively. Cyclic voltammetry curves and galvanostatic charge-discharge curves were teste on VMP3 Electrochemical Workstation (Bio-logic). Specific capacitances (Cs, Fg^{-1}) of materials were calculated based on the following formula: $Cs = I\Delta t/(m\Delta V)$, where I is discharge current, Δt is discharge time, m is the mass of active material and ΔV represents voltage window.

In the two-electrode symmetric supercapacitor configurations, the The specific capacitances were calculated by using the following equation: $Cs = I\Delta t/(m\Delta V)$, in which I is the constant discharge current, Δt is the time for a full discharge, m is the active material mass of two electrode and ΔV represents voltage drop on discharging. Energy density of the supercapacitor was calculated by $E = CsV^2/2$, where V is the cell operating voltage. The power densities of the device (P) were calculated from the following formula: $P = E/\Delta t$, where Δt is the discharge time.

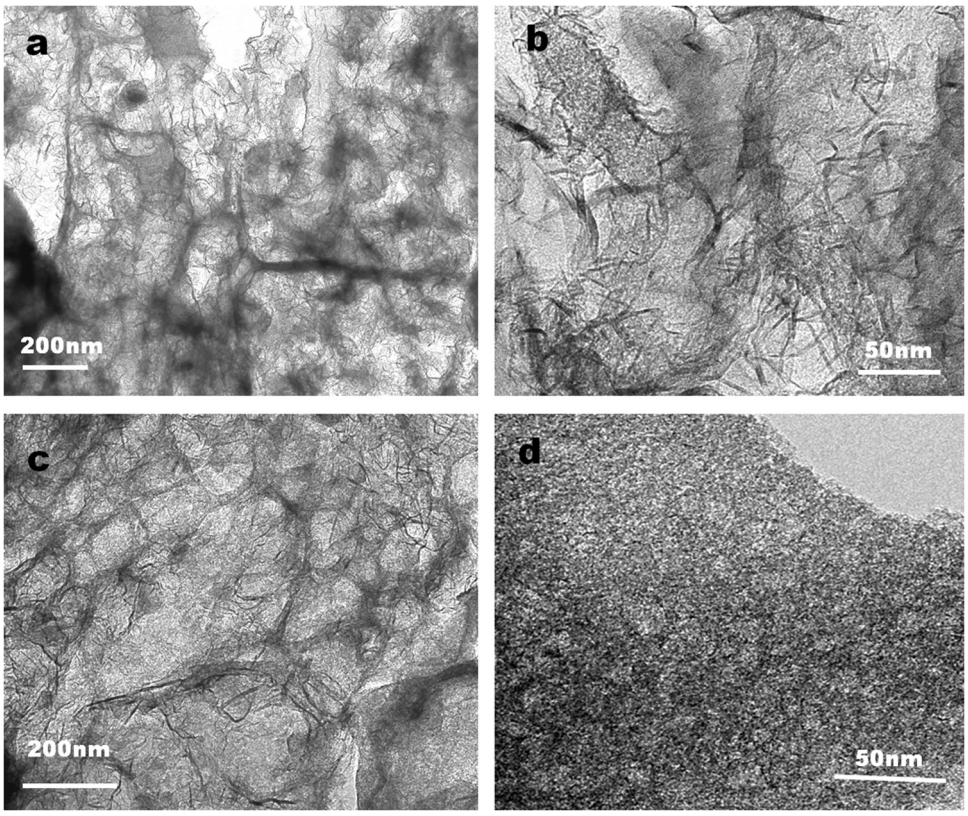

Fig. 3. TEM images of MTC (a and b) and MTC-KOH (c and d) with different magnifications.

Table 1
Physicochemical and electrochemical properties of MTC and MTC-KOH.

Samples	S_{BET} ($m^2\,g^{-1}$)	V_t ($cm^3\,g^{-1}$)	XPS analysis (at%)		C_s @ 0.5 Ag^{-1} (Fg^{-1})	C_s @ 30 Ag^{-1} (Fg^{-1})
			C	O		
MTC	1676	1.15	93.25	6.75	170	116
MTC-KOH	3175	1.93	98.25	1.75	275	120

Notes: S_{BET}: specific surface area, V_t: pore volume, C_s: specific capacitance.

3. Results and discussion

3.1. Synthesis process and structure characterization

The synthesis of hierarchical porous carbon (MTC) and highly porous carbon (MTC-KOH) are achieved by a simple templating carbonization and activation process. As illustrated in Fig. 1, aqueous precursor solution containing phenolic resin and Mg^{2+} undergo the drying and pyrolysis process to form nano-size MgO particles with various sizes. The nano-sized MgO particles give the resulting MTC sample with a hierarchical pore structure after washing. MTC further experiences a KOH activation process with mass ratio of 1:1 by which KOH could etch the carbon surface to yield MTC-KOH with abundant micropores.

Firstly, we investigate the influence of carbonization temperatures on the microstructure and porosity development of MTC. Fig. S1 shows the XRD patterns of MTC samples prepared under 900 °C (MTC), 800 °C (MTC-2) and 700 °C (MTC-3) from which all samples exhibit two broad diffraction peaks located at a 2θ value of ~25° and ~47°, which are associated with the graphite (002) plane and (100) plane [15]. More specifically, it can be found that decreasing the carbonization temperature will enlarge the full width at half maximum (FWHM) of (002) peaks. It is well-known that the stacking height (Lc) of graphitic structure is related to the FWHM of (002) plane ($Lc = 0.89\lambda/(FWHM002\cos\theta002)$), and higher FWHM results in more disordered packed structure from which it is indicated that low carbonization temperature should be adverse for developing the graphitic carbon framework. N_2 adsorption isotherms and XPS element analysis further reveal that decreasing carbonization temperature reduces porosity development and carbon atom contents mainly due to the incomplete carbonization of phenolic resin precursor (Fig. S2 and Table S1). Therefore, 900 °C was selected as the optimized carbonization temperature for obtaining MTC.

After carbonization, KOH activation was carried out at 900 °C to obtain MTC-KOH sample. The crystallinities of MTC and MTC-KOH were determined by XRD and Raman characterizations, which are shown in Fig. 2a and b, respectively. As a whole, both XRD and Raman analysis demonstrate the mainly amorphous structure of MTC and MTC-KOH, however, with different degree [15]. As shown in Fig. 2a, MTC exhibits two obvious diffraction peaks located at a 2θ value of ~25° and ~47° while the two graphite characteristic peaks almost disappear for MTC-KOH sample (Fig. 2a), revealing the microstructure difference between MTC and MTC-KOH. It should ascribe to the etching reaction between KOH and carbon framework that consumes the carbon framework and creates more pores. In addition, Raman spectra of MTC and MTC-KOH shown in Fig. 2b reveal a similar I_D/I_G ratio of MTC and MTC-KOH which suggests

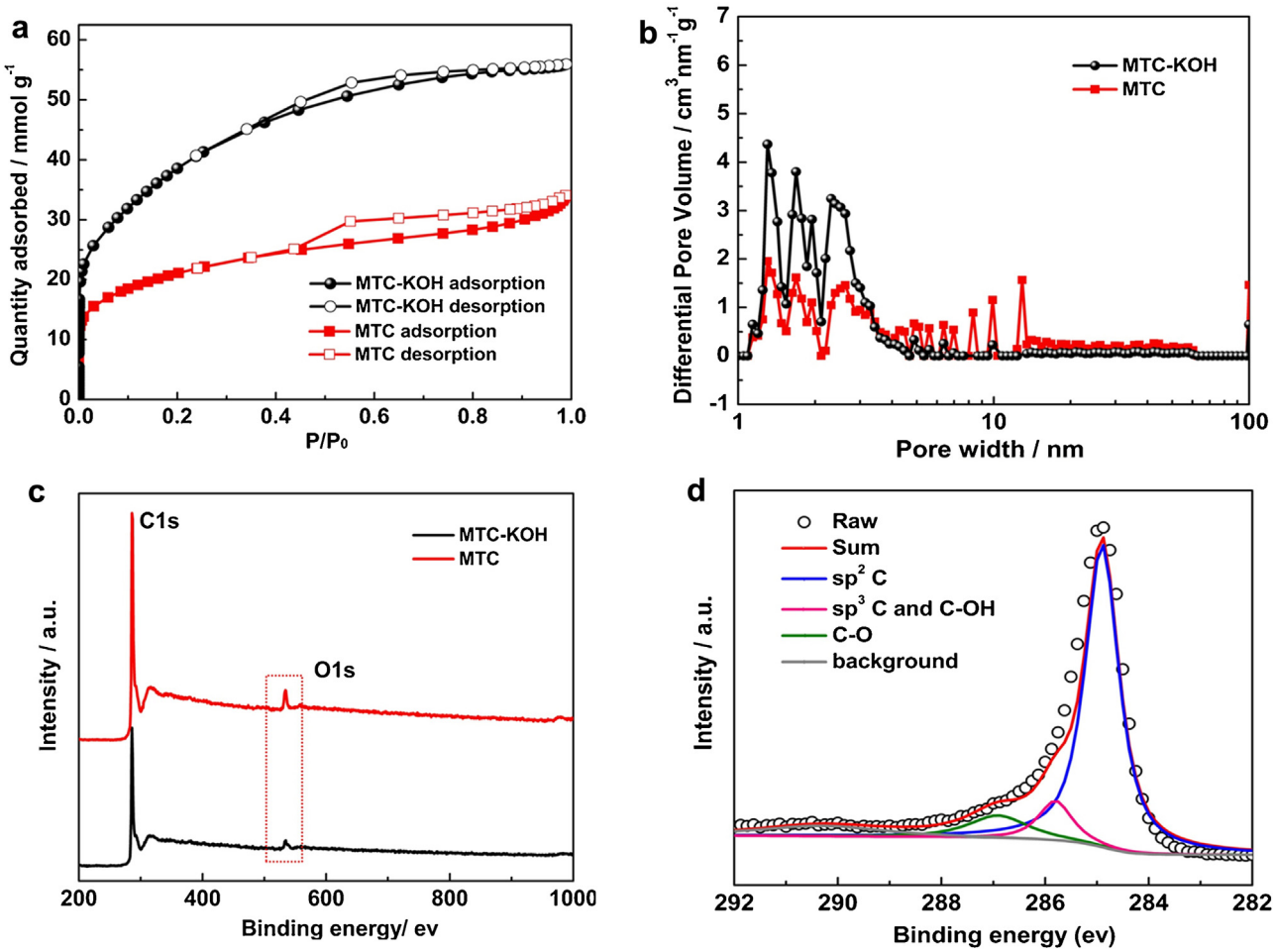

Fig. 4. (a) Nitrogen adsorption isotherms of MTC and MTC-KOH; (b) Pore size distributions of MTC and MTC-KOH; (c) XPS survey spectra of MTC and MTC-KOH; (f) C1s spectrum of MTC-KOH.

a similar distribution of disorder structure and graphitic structure between MTC and MTC-KOH.

Representative TEM images of MgO-templated porous carbon (MTC) and high purity carbon (MTC-KOH) are presented in Fig. 3a–d. Both MTC and MTC-KOH show amorphous structure with different scale nanopores embedding in the carbon framework. Specifically, MTC (Fig. 3a and b) shows a wire mesh-like with some large-scale pores dispersed in the carbon matrix, indicating that MgO template removal can generate large quantity of mesopores (identified by the scale bar). Comparatively, Fig. 3c and d shows the TEM images of MTC-KOH which demonstrates the dense micropores distributing uniformly in the carbon surface due to KOH etching.

N_2 adsorption/desorption isotherms and resulting pore size distributions were further investigated to reveal the pore configurations of MTC and MTC-KOH. As shown in Fig. 4a, MTC exhibits a combined I/IV type isotherms with an obvious hysteresis loop within the relative pressure P/P_0 of 0.4–1 indicating that micro-, meso,- and/or macropores coexist in MTC [17,18]. The resulting quenched solid density functional theory (NLDFT) based pore size distribution of MTC further demonstrates the hierarchical pore structure (Fig. 4b), including micropores centered around 1.5 and 1.8 nm as well as mesopores located from 2 to 15 nm. Such hierarchical pore configuration gives the BET surface area and total pore volume up to 1676 $m^2 g^{-1}$ and 1.15 $cm^3 g^{-1}$ (Table 1), respectively. It is well known that the hierarchical pore structure is beneficial to enhancing electrochemical process because the charge storage occurs predominately in the micropores and the larger pores provide fast mass-transport of electrolytes [19–21]. Compared with MTC, the adsorption/desorption isotherm and pore size distribution of MTC-KOH show highly developed small pores with pore size less than 3 nm (Fig. 4a and b). Impressively, the surface area and pore volume are up to 3175 $m^2 g^{-1}$ and 1.93 $cm^3 g^{-1}$, respectively (Table 1).

The chemical compositions of MTC and MTC-KOH were further investigated by X-ray photoelectron spectroscopy (XPS). Typical C1s and O1s signals can be observed in both MTC and MTC-KOH (Fig. 4c), but with different relative intensities. The O1s signal of MTC-KOH is relatively lower than that of MTC. Elemental analysis (Table 1) shows that O content in MTC-KOH is 1.75 atom%, much lower than that of MTC (6.75%). The high-resolution C1s XPS spectrum of MTC-KOH (Fig. 4d) can be deconvoluted into mainly three peaks representing *sp2* carbon (245 ± 0.2 eV), *sp3* carbon or C—OH (286 ± 0.2 eV), C—O (287 ± 0.2 eV) [22]. As expected, MTC-KOH exhibits a high percentage of sp^2 carbon component and low content of oxygen-containing groups. In contrast, MTC shows a relatively lower sp^2 carbon ratio and more oxygen species than those of MTC-KOH (Fig. S3). Above XPS results indicate that most of oxygen species in MTC sample can be etched out during the KOH activation process, leaving the carbon framework of MTC-KOH with ultrahigh carbon content (98.25 atom%). The high carbon atom ratio of MTC-KOH could ensure the structure stability during an electrochemical process, and thus may enhance the cycling stability.

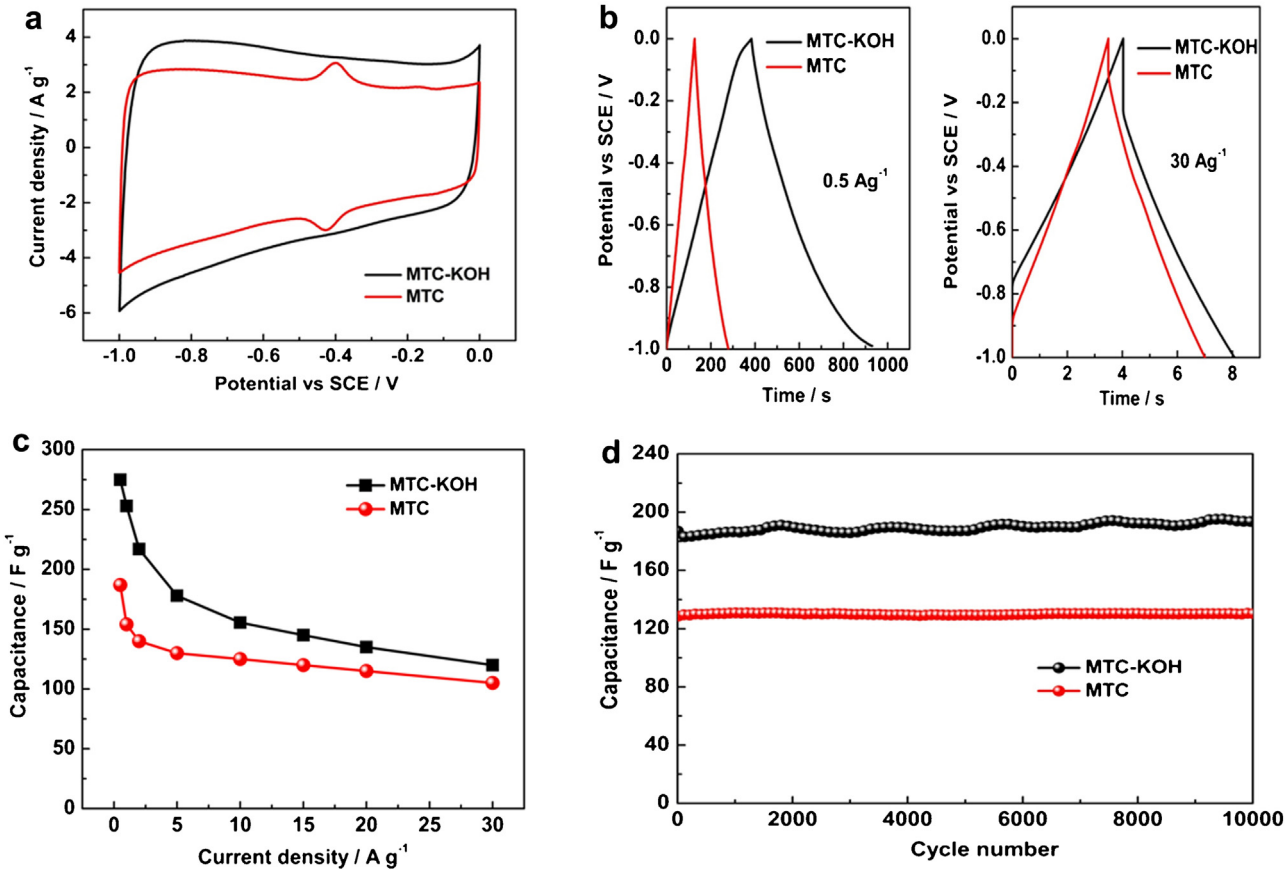

Fig. 5. Electrochemical performances of MTC and MTC-KOH in a three electrode configuration. (a) Cyclic voltammograms at a scan rate of 20 mV s^{-1}; (b) Charge-discharge profiles under different current densities; (c) Gravimetric capacitances at different charge-discharge current densities; (d) Cycling stability at 5 A g^{-1}.

3.2. Electrochemical performance in 6 M KOH in a three electrode system

MTC with hierarchical pore structure and MTC-KOH with simultaneously high surface area and carbon purity were further investigated as electrode materials for supercapacitors in a three-electrode system with 6 M KOH as an electrolyte. The electrochemical performances are presented in Fig. 5 and Fig. S4. CV curves in Fig. 5a clearly reveal the difference of capacitive process between MTC and MTC-KOH. In comparison with MTC which behave slight redox humps at around −0.4 V, the CV curve of MTC-KOH maintains a perfect electrical double-layer capacitor behavior, indicating no pseudocapacitive effect [16]. Undoubtedly, the redox characteristic in the of MTC must originate from O-doping while MTC-KOH possessing ultra high carbon purity shows no pseudo-capacitive characteristic.

The galvanostatic charge-discharge curves for MTC and MTC-KOH at low rate and high rate are shown in Fig. 5b. At a low current density of 0.5 A g^{-1}, MTC shows a specific capacitance of 170 F g^{-1} while MTC-KOH exhibits a much higher capacitance of 275 F g^{-1}. However, at a high rate of 30 A g^{-1}, the capacitance gap between MTC (116 F g^{-1}) and MTC-KOH (120 F g^{-1}) is lessened and MTC displays a smaller IR drop than MTC-KOH (Fig. 5b). This could be explained by the different pore structures of MTC and MTC-KOH. Compared with MTC, the higher surface area of MTC-KOH ensure sufficient ion storage areas and therefore exhibit high specific capacitance at low current density. However, MTC featuring a hierarchical pore structure can achieve fast ion transfer reflecting in the small IR drop and excellent rate performance (also seen in Fig. 5c). In addition, both MTC and MTC-KOH display outstanding cycling stability that there is almost no capacitance decay after 10,000 cycles (Fig. 5d).

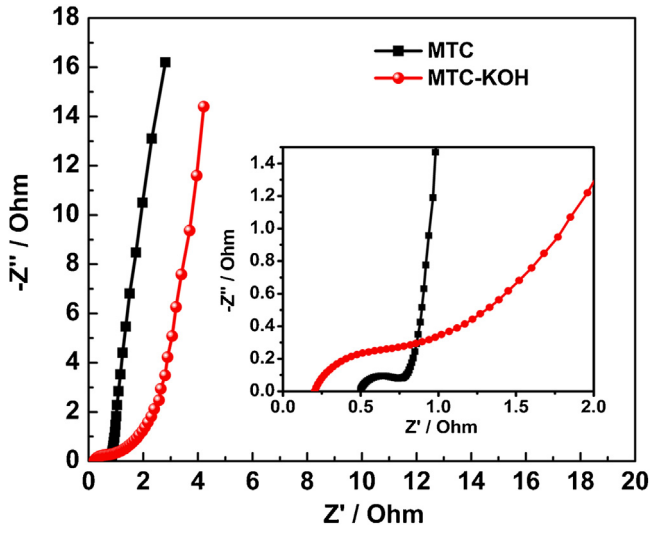

Fig. 6. Nyquist plots of MTC and MTC-KOH in 6 M KOH.

Electrochemical impedance spectroscopy was further performed to investigate the ion- and electron-transport kinetics of MTC and MTC-KOH. Fig. 6 shows the Nyquist plots of the MTC and MTC-KOH electrodes in 6 M KOH. The straight line in the low-frequency region and the semicircle in the high frequency region indicate a typical capacitive behavior [21,23]. The intrinsic Ohmic resistance (the first intercept along the real axis) of

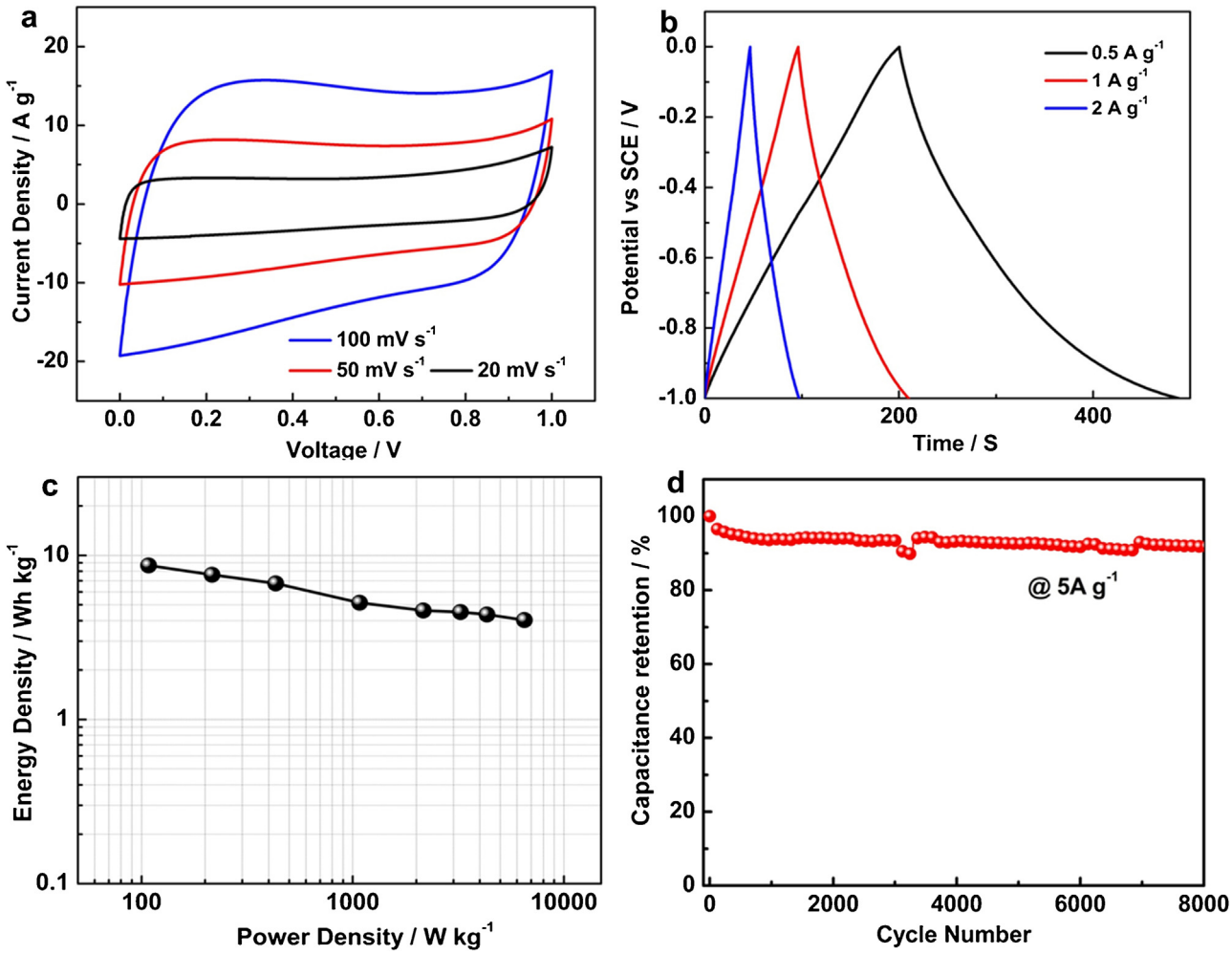

Fig. 7. Electrochemical performances of MTC-KOH based symmetric supercapacitor. (a) Cyclic voltammograms under different scan rate; (b) Charge-discharge profiles under different current densities; (c) Ragone plot; (d) Cycling stability at 5 A g^{-1}.

the MTC electrode is slightly higher than that of MTC-KOH. However, by extrapolating the vertical portion to the real axis, the MTC electrode shows a much smaller equivalent series resistance (ESR) of ~0.5 Ω than that of MTC-KOH (~1.6 Ω), which confirms the lower contact resistance [21]. Moreover, MTC-KOH shows a larger charge transfer resistance (the diameter of the semicircle) than that of MTC which should stem from the much low heteroatom contents. As known, oxygen and/or nitrogen doping could help to enhance the surface wettability of carbon materials and endow fast electrolyte approaching and transfer within electrodes. MTC-KOH shows much low oxygen content and high carbon purity, and thus enables the constructed electrode with increased hydrophobicity and decreased wettability which reflects on the larger charge transfer resistance than MTC. Furthermore, the straight line in the low-frequency region of MTC electrode exhibits an increasing slope as compared with the MTC-KOH electrode, indicating promoted ion transportation [23]. The EIS results further explain the different rate performances of MTC and MTC-KOH.

3.3. Electrochemical performances of symmetric supercapacitor

To validate the device performance of MTC-KOH with high specific capacitance, further measurements were conducted in a two electrode symmetric cell configuration. Rectangular shapes in CV curves (Fig. 7a) and triangular shapes in galvanostatic charge-discharge curves (Fig. 7b) indicate a typical EDLC behavior [24]. Ragone plot (Fig. 7c) further reveals the excellent capacitive performance of MTC-KOH, which gives energy densities of 8.68 Wh kg^{-1} and 4.03 Wh kg^{-1} with the corresponding power densities of 108 W kg^{-1} and 6.49 kW kg^{-1}, respectively. To demonstrate the cycling stability of the MTC-KOH electrode, charge-discharge cycles were measured at a constant current density of 5 A g^{-1} (Fig. 7d). The specific capacitance remains >90% of the initial capacitance after 8000 cycles, indicating a long lifespan. To sum up, the excellent supercapacitive performance of MTC-KOH must result from the combined structure advantages of high surface area and high carbon purity.

4. Conclusion

In summary, we have developed a simple and inexpensive templating carbonization coupling with KOH activation method to stepwise synthesize MgO-templated porous carbon (MTC) and highly porous carbon (MTC-KOH). As electrode materials for supercapacitors, MTC exhibits good rate performance due to the hierarchical pore configuration and MTC-KOH with highly developed microporous structure shows high capacitance and cycling stability, delivering 275 F g^{-1} at 0.5 A g^{-1} and 120 F g^{-1} at 30 A g^{-1}. Moreover, MTC-KOH based symmetric supercapacitor delivers high energy densities, power densities and long lifespan. The excellent supercapacior performance of MTC-KOH is due to the synergetic advantages of large surface area and ultra high carbon purity.

Acknowledgement

This research was financially supported by the National Natural Science Foundation of China (Grant No. 51376054).

Appendix A. Supplementary data

Supplementary data associated with this article can be found, in the online version, at http://dx.doi.org/10.1016/j.apsusc.2016.06.176.

References

[1] Y.W. Zhu, S. Murali, M.D. Stoller, K.J. Ganesh, W.W. Cai, P.J. Ferreira, et al., Science 332 (2011) 1537–1541.
[2] J. Yan, Q. Wang, T. Wei, Z.J. Fan, Adv. Energy Mater. 4 (2014) 1300816.
[3] K. Yan, L.B. Kong, L.W. Shen, Y.H. Dai, M. Shi, B. Hu, et al., Appl. Surf. Sci. 28 (2016) 850–861.
[4] P. Simon, Y. Gogotsi, Nat. Mater. 7 (2008) 845–854.
[5] H. Chen, F. Wang, S.S. Tong, S.L. Guo, X.M. Pan, Appl. Surf. Sci. 16 (2012) 6097–6102.
[6] Z. Chen, J. Wen, C.Z. Yan, L. Rice, H. Sohn, M.Q. Shen, et al., Adv. Energy Mater. 1 (2011) 551–556.
[7] J. Lee, J. Kim, T. Hyeon, Adv. Mater. 16 (2006) 2073–2094.
[8] P. Strubel, S. Thieme, T. Biemelt, A. Helmer, M. Oschata, J. Brckner, et al., Adv. Funct. Mater. 25 (2015) 287–297.
[9] D.S. Jung, T.H. Hwang, J.H. Lee, H.Y. Koo, R.A. Shakoor, R. Kahraman, et al., Nano Lett. 14 (2014) 4418–4425.
[10] T. Morishita, T. Tsumura, M. Toyoda, J. Przepiorski, A.W. Morawski, H. Konno, et al., Carbon 48 (2010) 2690–2707.
[11] X. He, H. Zhang, H. Zhang, X. Li, N. Xiao, J. Qiu, J. Mater. Chem. A 2 (2014) 19633–19640.
[12] C.J. Cui, W.Z. Qian, Y.T. Yu, C.Y. Kong, B. Yu, L. Xiang, et al., J. Am. Chem. Soc. 136 (2014) 2256–2259.
[13] W. Zhang, Z. Huang, G. Cao, F. Kang, Y. Yang, J. Phys. Chem. Solids 73 (2012) 1428–1431.
[14] G.W. Yang, H.Y. Han, T.T. Li, C.Y. Du, Carbon 50 (2012) 3753–3765.
[15] X.Y. Chen, C. Chen, Z.J. Zhang, D.H. Xie, J. Mater. Chem. A 1 (2013) 10903–10911.
[16] L. Sun, C.G. Tian, Y. Fu, Y. Yang, J. Yin, L. Wang, H.G. Fu, Chem. Eur. J. 20 (2014) 564–574.
[17] L. Qie, W.M. Chen, H.H. Xu, X.Q. Xiong, Y. Jiang, F. Zou, et al., Energy Environ. Sci. 6 (2013) 2497–2504.
[18] X.L. Yan, X.J. Li, Z.F. Yan, S. Komarneni, Appl. Surf. Sci. 30 (2014) 306–310.
[19] W.D. Geng, F.W. Ma, G. Wu, S.J. Song, J.F. Wan, D. Ma, Electrochim. Acta 191 (2016) 854–863.
[20] D.W. Wang, F. Li, M. Liu, G.Q. Lu, H.M. Cheng, Angew. Chem. Int. Ed. 47 (2008) 373.
[21] J. Zhao, H.W. Lai, Z.Y. Lye, Y.F. Jiang, K. Xie, X.Z. Wang, et al., Adv. Mater. 27 (2015) 3541–3545.
[22] X.L. Li, H.L. Wang, J.T. Robinson, H. Sanchen, G. Diankov, et al., J. Am. Chem. Soc. 131 (2009) 15939–15944.
[23] I.I.G. Inal, S.M. Holmes, A. Banford, Z. Aktas, Appl. Surf. Sci. A 1 (2015) 696–703.
[24] C. Long, J.L. Zhuang, Y. Xiao, M.T. Zheng, H. Hu, H.W. Dong, J. Power Sources 310 (2016) 145–153.